Journal of Applied Sciences 6 (10): 2209-2216, 2006
ISSN 1812-5654

Tuning Semiconductor Laser Diode Lasing Frequency and Narrowing the Laser Linewidth Using External Oscillating Driving Field

H.S. Ashour
Department of Physics, Al-Azhar University-Gaza, Palestinian Authority, Palestine

Abstract: In this study, we propose a new method to tune the semiconductor laser lasing frequency and reducing the laser linewidth using an external deriving field. We redeveloped Floquet S-matrix which determines the transmission probabilities and the shape and position of the induced quasibound state, which accumulated incident electrons. We explored the S-matrix numerically for various system parameters. We found that the oscillating field amplitude V_1 plays a curial rule in defining the profile of electrons accumulations in the quasibound state and the field's strength made sift the position of the quasibound state. This sift in the bound state energy due field's strength is used to tune the lasing frequency and the output of the semiconductor laser linewidth is improved by changing the field's amplitude the deriving field. By narrowing down the electron accumulations profile the laser linewidth would be narrower.

Key words: Laser, tunable, semiconductor laser, laser linewidth

INTRODUCTION

Tunable lasers are different than the traditional lasers because they can change their output frequency, color, in a given spectral range. These quantum devices found numerous applications in many diverse fields. Among the fields that employ tunable lasers are: laser cooling, atomic physics, communication, imaging, medicine, remote sensing, etc. Tunable laser, were discovered by Sorokin and Lankard (1966) and Schafer *et al*. (1966), was a dye laser. A significant advance toward emission control was provided by Peterson *et al*. (1970). However, these lasers were not compact and required a large two-dimensional diffraction grating. Resonator laser designed to yield tunable narrow linewidth emission in compact and improved configurations are the grazing-incident cavities (Shoshan *et al*., 1997; Littman and Metcalf, 1978; Littman, 1984) and the multiple-prism grating oscillators (Durate and Piper, 1980, 1981, 1984). These cavity designs have been successful in tuning and frequency narrowing in gas lasers, solid-state lasers and semiconductor lasers.

Semiconductor lasers are vastly used in Dense Wavelength Division Multiplexing (DWDM) networks, including wavelength conversion, optical routing and multi-wavelength sparing. Many techniques currently being investigated to produce such lasers (Hong *et al*., 1998; Mason *et al*., 1999; Vakhshoori *et al*., 1999; Zorabedian, 1995; Jerman *et al*., 2001): external cavity diode lasers (ECL) offer significant advantages, including wide tuning ranges, high output power, narrow linewidths with good side mode suppression and accurate wavelength control. These devices are widely used in test equipment, but the size and complexity of the optomechanical assemblies have limited their use in optical Networks (Shoshan *et al*., 1997). The use of silicon MEMS, Micro-Electro-Mechanical Systems, to perform the mechanical tuning functions makes it possible to greatly reduce the size and complexity of the devices and combining the ECL and an etalon wavelength locker (WLL) in the same package results in a compact, robust device suitable for use in optical networks (Zorabedian, 1995).

Wenjun and Reichl (1999, 2000) Moskalets and Büttiker (2002a, b) Al-Sahhar *et al*. (2005) and Tang *et al*. (2003) studied the electron scattering through time periodic potential well using Floquet S-matrix. In their study they found that the oscillator-induced quasibound states can accumulate electrons and give rise to electrons interchannel transitions at resonance. The transmission resonances result from the interaction of electrons with oscillating field. Also, the applied field causes the bound state of the quantum well to be sifted by a certain amount because of this interaction.

THEORY

Bound state: For GaAs/$Al_xGa_{1-x}As$ finite barrier quantum well, the potential is given by (Chuang, 1995)

$$V(x)=\begin{cases} V_0 & |x|\geq \frac{L}{2} \\ 0 & |x|<\frac{L}{2} \end{cases} \quad (1)$$

The Schrödinger wave equation is

$$\left[-\frac{d}{dx}\frac{1}{m}\frac{d}{x}+V(x)\right]\psi(x)=E\psi(x) \quad (2)$$

Where $m=m_1^*$ in the well region and $m=m_2^*$ in the barrier region. Here, we are going to consider the bound state solution which have energies in the range between 0 and V_0.

Solving Eq. 2 in the well and barrier regions and applying the boundary conditions, we can find the eigenenergies E.

In general, the solutions for quantized eigenenergies can be obtained directly using,

$$\left(k\frac{L}{2}\right)^2+\frac{m_1^*}{m_2^*}\left(\alpha\frac{L}{2}\right)^2=\frac{2m_1^*V_0}{\hbar^2}\left(\frac{L}{2}\right)^2 \quad (3)$$

and

$$\alpha\frac{L}{2}=\frac{m_2^*}{m_1^*}k\frac{L}{2}\tan\left(k\frac{L}{2}\right) \text{ for even solution} \quad (4)$$

$$\alpha\frac{L}{2}=-\frac{m_2^*}{m_1^*}k\frac{L}{2}\cot\left(k\frac{L}{2}\right) \text{ for odd solution} \quad (5)$$

Where $\alpha=-\frac{m_2^*}{m_1^*}k\cot\left(k\frac{L}{2}\right)$ and $k=\frac{\sqrt{2m_1^*E}}{\hbar}$. Equation (3-5) can be solved either numerically or graphically to obtain the bound state eigenenergy.

Floquet scattering: When an external oscillating field with frequency ω and amplitude V_1 is applied on the GaAs quantum well, sandwiched between two layers of AlGaAs as in Fig. 1, the Schrödinger wave equation is given by

$$i\hbar\frac{\partial}{\partial t}\psi(x,t)=-\frac{\hbar^2}{2m_1^*}\frac{\partial^2}{\partial^2 x^2}\psi(x,t)+V(x,t)\psi(x,t) \quad (6)$$

Thus m_1^* is the electron's effective mass in the well region and V(x, t) is the total field given by

$$V(x,t)=\begin{cases}0 & x>L/2\\ V_0+V_1\cos(\omega t) & -L/2<x<L/2\\ 0 & -L/2>x\end{cases} \quad (7)$$

Thus L is the quantum well width and V_1 is the field strength.

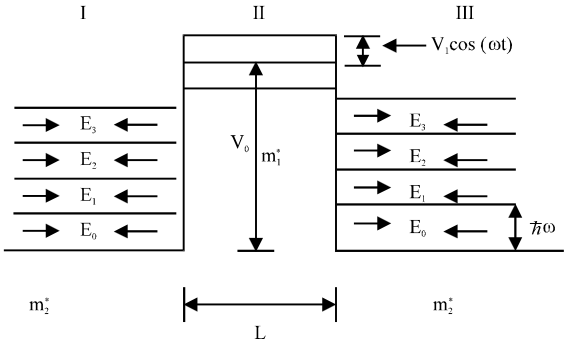

Fig. 1: Floquet scattering model. The incoming electrons and back scattered electrons in channels are spaced by field strength $\hbar\omega$. Floquet channels are spaced according to $E_n=E_0+n\hbar\omega$ $[n\in[0,\infty)]$. The evanescent mode exits but not included in the figure

In this treatment, we neglected electron-electron interaction and we assume the temperature is low enough so that electron-phonon interaction can be neglected as well. We assumed the scattering of electrons mainly form the geometrical structure of the potential.

According to Floquet theorem Eq. 6 has a solution of the form (Al-Sahhar *et al*., 2005)

$$\psi_F(x,t)=e^{-iE_Ft/\hbar}\phi(x,t) \quad (8)$$

Thus E_F is the Floquet energy and to be determined from the boundary conditions. We need to solve Schrödinger wave Eq. (6) for each layer then apply the boundary conditions between the adjacent layers. The Floquet state, $\Psi_{II}(x, t)$, inside the oscillating quantum well is given by:

$$\psi_{II}(x,t)=e^{-iE_Ft/\hbar}\sum_{n=-\infty}^{\infty}\sum_{m=-\infty}^{\infty}\left(a_m e^{iq_m x}+b_m e^{-iq_m x}\right)J_{n-m}\left(\frac{V_1}{\hbar\omega}\right)e^{-in\omega t} \quad (9)$$

Thus a_m and b_m are constant coefficients to be determined from the boundary conditions and q_m can be found from the following relation

$$\frac{\hbar^2 q_m^2}{2m_1^*}=E_F+m\hbar\omega-V_0 \quad (10)$$

When a beam of electrons is incident on the oscillating quantum well the electrons will be scattered inelastically into Floquet side bands. In order to able to apply the boundary conditions between the oscillating quantum

well and the adjacent regions the wave function outside the quantum well must consist of many Floquet side bands. The solution of Schrödinger wave equation outside the oscillating quantum well, in region I and III, is given by

$$\psi^{I}(x,t)=\sum_{n=-\infty}^{\infty}\left(A_n^i\, e^{(ik_n x-iE_n t/\hbar)}+A_n^o\, e^{(-ik_n-iE_n t/\hbar)}\right) \quad (11)$$

$$\psi^{II}(x,t)=\sum_{n=-\infty}^{\infty}\left(B_n^i\, e^{(-ik_n x-iE_n t/\hbar)}+B_n^o\, e^{(ik_n-iE_n t/\hbar)}\right) \quad (12)$$

Thus A_n^i and B_n^i are the probability amplitudes of the incoming waves from the left and right, respectively, while A_n^o and B_n^o are the probability amplitudes of the outgoing waves. The incoming and outgoing waves are divided into different zones according to channel index n: $E_n = E_0 + n\hbar\omega$, where E_0 is the Floquet energy of the propagating mode with the lowest energy (Wenjun and Reichl, 1999; Moskalets and Büttiker, 2002a). Also, it is important to mention that $k_n=\sqrt{2m_2^* E_n/\hbar^2}$ where m_2^* is the electron's effective mass in the AlGaAs layers. But, when $E_n<0, k_n=\sqrt{2m_2^* E_n/\hbar^2}$ is imaginary, such a mode will not propagate and is called evanescent mode.

The Floquet Scattering matrix can be obtained by; the derivation is analogous to (Wenjun and Reichl, 1999; Al-Sahhar *et al*., 2005) but needs some tedious algebra, using Eq. (9), (11) and (12). That is

$$\begin{pmatrix}A^o\\B^o\end{pmatrix}=S\begin{pmatrix}A^i\\B^i\end{pmatrix} \quad (13)$$

The S matrix consists of all the probability amplitudes which connect the coefficients A_n^i, B_n^i to the coefficients. The structure of the S-matrix is

$$S=\begin{pmatrix}M_{AA} & M_{AB}\\ M_{BA} & M_{BB}\end{pmatrix} \quad (14)$$

Where the elements M_{AA}, M_{AB}, M_{BA} and M_{BB} are given by

$$M_{AA}=\frac{1}{2}\begin{Bmatrix}M_c^+\cdot\left[\left(M_s^+\right)^{-1}+\left(M_s^-\right)^{-1}\right]+\\ M_c^-\left[\left(M_s^+\right)^{-1}-\left(M_s^-\right)^{-1}\right]\end{Bmatrix}\cdot M_r - M_i \quad (15.a)$$

$$M_{AB}=\frac{1}{2}\begin{Bmatrix}M_c^+\cdot\left[\left(M_s^+\right)^{-1}-\left(M_s^-\right)^{-1}\right]+\\ M_c^-\left[\left(M_s^+\right)^{-1}+\left(M_s^-\right)^{-1}\right]\end{Bmatrix}\cdot M_r \quad (15.b)$$

$$M_{BA}=\frac{1}{2}\begin{Bmatrix}M_c^-\cdot\left[\left(M_s^+\right)^{-1}+\left(M_s^-\right)^{-1}\right]+\\ M_c^+\left[\left(M_s^+\right)^{-1}-\left(M_s^-\right)^{-1}\right]\end{Bmatrix}\cdot M_r \quad (15.c)$$

$$M_{BB}=\frac{1}{2}\begin{Bmatrix}M_c^-\cdot\left[\left(M_s^+\right)^{-1}-\left(M_s^-\right)^{-1}\right]+\\ M_c^+\left[\left(M_s^+\right)^{-1}+\left(M_s^-\right)^{-1}\right]\end{Bmatrix}\cdot M_r - M_i \quad (15.d)$$

Where

$$M_s^{\pm}=\begin{bmatrix}\left(\frac{m_1^*}{m_2^*}k_n+q_m\right)e^{-iq_m L/2}\pm\\ \left(\frac{m_1^*}{m_2^*}k_n-q_m\right)e^{iq_m L/2}\end{bmatrix}J_{n-m}\left(\frac{V_1}{\hbar\omega}\right) \quad (16.a)$$

$$M_r=2\frac{m_1^*}{m_2^*}k_n e^{-ik_n L/2}\delta_{n,m} \quad (16.b)$$

$$M_c^{\pm}=e^{-i(k_n\pm q_m)L/2}J_{n-m}\left(\frac{V_1}{\hbar\omega}\right) \quad (16.c)$$

$$M_i=e^{-ik_n L}\delta_{n,m} \quad (16.d)$$

In the S-matrix each element gives the probability amplitude of electron scattered from Floquet sideband m to sideband n [n, m ∈ (-∞, ∞)].

The S-matrix of the incoming and outgoing Floquet sidebands in the following form

$$S=\begin{pmatrix}r_{00} & r_{01} & . & . & t'_{00} & t'_{01} & . & .\\ r_{10} & r_{11} & . & . & t'_{10} & t'_{11} & . & .\\ . & . & . & . & . & . & . & .\\ . & . & . & . & . & . & . & .\\ t_{00} & t_{01} & . & . & r'_{00} & r'_{01} & . & .\\ t_{01} & t_{11} & . & . & r'_{10} & r'_{11} & . & .\\ . & . & . & . & . & . & . & .\\ . & . & . & . & . & . & . & .\end{pmatrix} \quad (17)$$

Where r_{nm} and t_{nm} are the reflection and transmission coefficients, respectively, for modes incident from left; r'_{nm} and t'_{nm} and for modes incident from right; r_{nm} and t_{nm}. The other modes like $t_{-1,0}$, $r_{-1,0}$ in the S-matrix, does not appear in Eq. 17, correspond to probability amplitude describing an electron with incident energy E_0 being scattered into the evanescent mode $E_{-1}=E_0-\hbar\omega$. In other word, the electron lost a quanta $\hbar\omega$ upon its interaction with the oscillating quantum well.

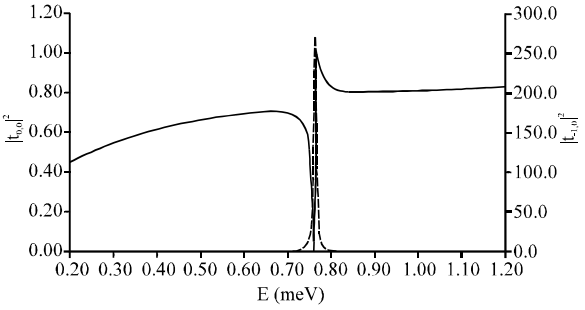

Fig. 2: The transmission coefficient T as a function of incident energy for the list above system parameters, the solid line. The secondary axis shows the accumulation of electrons in quasi bound state

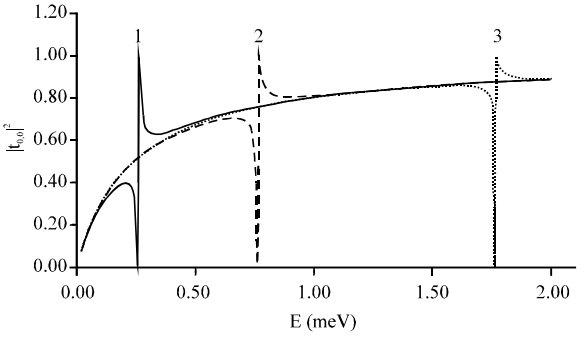

Fig. 3a: The transmission coefficient T as function of incident energy for different oscillating field energies. Curve 1 with $0.5\,\hbar\omega$, curve 2 with $\hbar\omega$ and curve 3 with $\mathbf{1.5\,\hbar\omega}$

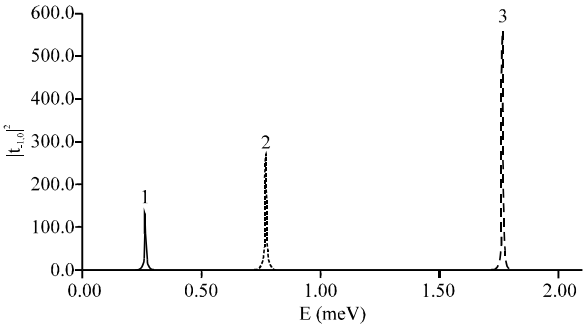

Fig. 3b: The accumulation of electrons in the quasi bound state induced by the oscillating driving field with energies listed in Fig. 3a

From the scattering S-matrix the total transmission coefficient can be obtained

$$T = \sum_{n=0}^{\infty}\sum_{m=0}^{\infty}\frac{k_n}{k_m}\left|t_{nm}\right|^2 \qquad (18)$$

According Landuar-Büttiker formula (Wenjun and Reichl, 1999, 2000; Moskalets and Büttiker, 2002a,b) the total conductance, which can be measured experimentally, is given by:

$$G = \frac{2e^2}{h}T \qquad (19)$$

In the numerical simulation, the minimum number of sidebands, channels, is determined by the strength of the oscillation according to (Wenjun and Reichl, 1999; Moskalets and Büttiker, 2002a)

$$N \cong V_1/\hbar\omega \qquad (20)$$

The numerical routine showed some deviations from Eq. (20). We took this deviation into account by monitoring the probability of each channel. Then, we decide if the number of channels included is enough or not. In Fig. 2, we numerically find the transmission trough oscillating quantum well using the following parameters; V_0 = -20 meV, V_1 = 5 me V, L = 10 A°, $m_1^* = 0.067m_e$, $m_2^* = 0.0916$ for x = 0.3 and $\hbar\omega = 1$ meV. According to Eq. 20, we need 5 sidebands to take into account. So, the over all sidebands in the scattering pattern is 11: 5 above the incident energy and 5 below the incident energy. The energy of each sideband is given $E_n = E_0 + n\hbar\omega$ with $n = 0,\pm1,....\pm N$ and N = 5.

As can be seen in Fig. 2, the transmission has a dip followed by a sharp increase in the transmission at certain energy value. This is called asymmetric Fano resonance (Wenjun and Reichl, 1999) at E = 0.762 meV, $E = \hbar\omega - |E_B| \approx 0.762$ meV, where E_B is the bound state energy when V_1 = 0 which equals -0.238 meV. This dip is occurred when the difference between the incident electron energy and the bound state us equal to $\hbar\omega, 2\hbar\omega, \ldots$.

In Fig. 3, we explore the effect of the oscillating frequency, $\hbar\omega$, on the transmission pattern. The number of channels included in this figure according to Eq. 20. In Fig. 3a, we plot the transmission coefficient versus electron's incident energy with different values of $\hbar\omega$. The first curve resonance occurs at 0.58 meV with field incident energy is $0.5\ \hbar\omega$, the second curve resonance occurs at 0.762 me V when the incident field energy is $\hbar\omega$ and the third curve resonance occurs at 1.76 meV for the incident field energy $1.5\ \hbar\omega$. In Fig. 3b, we show the electrons accumulation in the quasibound state which occurs where the resonance occurred. Notice, the higher the energy of the oscillating filed energy the higher the quasibound states can accumulate electrons.

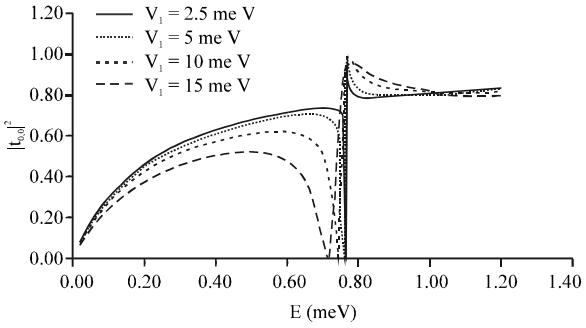

Fig. 4a: The transmission coefficient T as function of incident energy for different oscillating field amplitudes listed in the Fig. legends

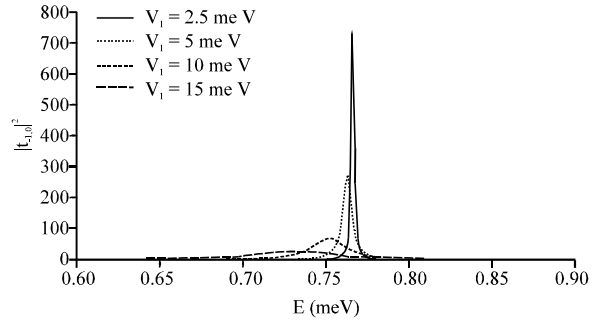

Fig. 4b: The accumulation of electrons in the quasi bound state induced by the oscillating driving field amplitudes listed in the Fig. legends

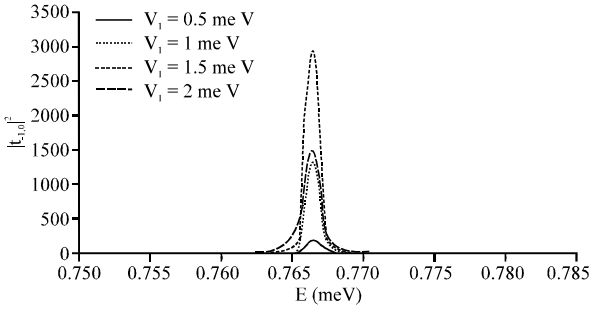

Fig. 4c: The accumulation of electrons in the quasi bound state induced by the oscillating driving field amplitudes listed in the Fig. legends

In Fig. 4, we study the effect of the strength of the oscillating field, V_1. The number of channels included to reach this figure is according to Eq. 20, which ranges between seven to fifteen channels. The system parameters are V_0 = -20 meV, L = 10 A°, m_1^* = 0.067m_e, m_2^* = 0.0916 and $\hbar\omega$ = 1 meV. In Fig. 4a, we plot the transmission T versus the incident electron energy but with different amplitudes of the incident deriving field. We

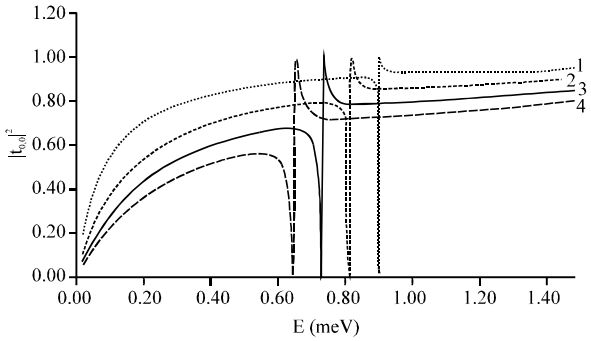

Fig. 5a: The transmission coefficient T as function of incident energy for different effective masses for the barrier region. Curve 1 with $m_2^* = 0.5m_1^*$, curve 2 with $m_2^* = m_1^*$, curve 3 with $m_2^* = 1.5m_1^*$

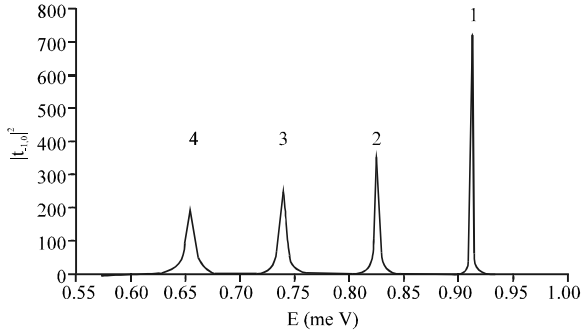

Fig. 5b: The accumulation of electrons in the quasi bound state induced by the oscillating driving field amplitude with different effective masses in the barrier region listed in Fig. 5a

notice that asymmetric Fano resonance widen with V_1 increase. In Fig. 4b, we plot the accumulation of electrons in the quasibound state. The quasibound state is sharper when V_1 is small but it is broader when V_1 takes high values. This broad quasibound state gives high uncertainty in electron's energy. Ironically, the increase in the field's amplitude leads to broad quasibound state, Fig. 4b. In Fig. 4c, we explore the possible amplitude values which can be effective in accumulating electrons in the quasibound state. We found that when the oscillating field amplitude is increased the number of electrons piled in the quasibound state is increased and the quasibound state getting sharper but to certain limit, for the system parameters listed earlier is 1.5 meV. When this certain limit is exceeded the quasibound state accumulates fewer electrons than before and become broader.

In Fig. 5, we study the effect of the electron's effective mass difference between the barrier and well regions. We have used the following system parameters:

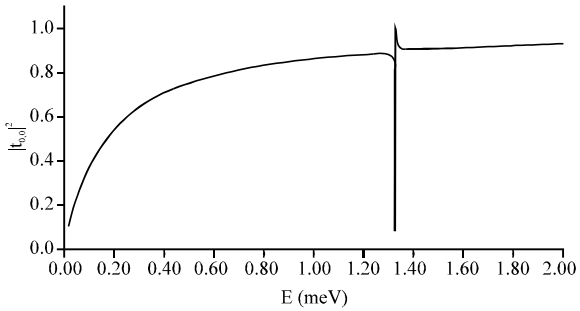

Fig. 6a: The transmission coefficient T as function of incident energy for the following system parameters: $V_0 = -20$, $m_1^* = 0.0916m_e$, $m_2^* = 0.067m_e$, $\hbar\omega = 1.5meV$ and $V_1 = 2.5meV$

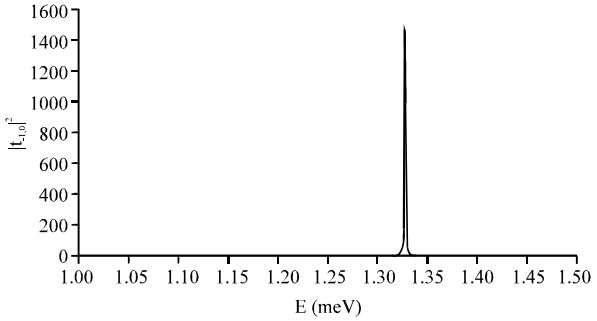

Fig. 6b: The accumulation of electrons in the quasi bound state induced by the oscillating driving field amplitude with system parameters

V_0 = -20 meV, V_1 = 5 meV, L = 10 A°, m_1^* = 0.067 m_e, $\hbar\omega$ = 1 me V and with the barrier effective masses, m_2^* = {0.5,1,1.5,2} m_1^*. In Fig. 5a, we study the effect of the effective masses on the transmission T. The transmission resonance occurs at different electron energy when the effective masses changes. This change should be at no surprise for us if we look back at Eq. (3-5). In Fig. 5b, the electrons accumulation in the quasibound states is the highest and sharpest when the effective mass of the barrier region is lower than the effective mass of the well region. But, when the effective mass of the barrier is higher than that of the well, the electron accumulation starts to spread over a quite wide energy values. This spread gives a quite large uncertainty in the electron energy.

Here, we will utilize all the information gained from the figures. If we want a sharp and high accumulation for electrons, we need to use high values for oscillating field energy, $\hbar\omega$, the field amplitude is law and the effective mass of the well region is higher than the barrier region. The position of the quasibound state can be shifted by changing the effective masses or the field energy, but once the device is fabricated the only parameter we control over is the field energy. In Fig. 6a and b, we plot the transmission and the electron accumulations for the following system parameters: V_0 = -20 meV, m_1^* = 0.0916 m_e, m_2^* = 0.067 m_e, $\hbar\omega$ = 1.5 meV and V_1 = 2.5 meV.

TUNING THE SCL

We describe a simplest form of semiconductor laser diode (Chuang, 1995; Büttiker, 1986; Landauer, 1989; Yariv, 1989; Verdeyen, 1995) and the references therein. The semiconductor laser structured from a thin (0.1 ~ 0.2 μm) region of GaAs which is sandwiched between two regions of $Ga_{1-x}Al_xAs$ of opposite doping forming a double heterojunction. In Fig. 7 shows the energy band structure of a diode laser. In Fig. 7, shows the conduction and valance band edges in heterojunction diode at full forward bias. In this structure a potential well of electrons of height ΔE_c which coincides spatially with a well for holes of height ΔE_v. In other word, we have direct band gap structure which is recommended for light generation devices. Under forward bias with $eV_a \sim E_g$, where V_a is the applied voltage and E_g is the energy gap, the large densities of injected electrons from the n side and holes from the p side in the well, causes the inversion condition, given by

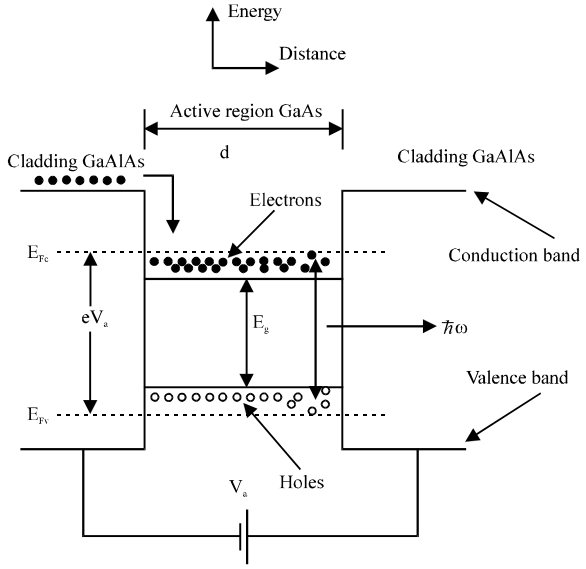

Fig. 7: Schematic diagram of semiconductor laser diode. The conduction and valence band edges under positive bias in a double heterojunction GaAlAs/GaAs/GaAlAs laser diode. The black circles is electrons and the hollow circle is the holes

$$E_{Fc} - E_{Fv} > \hbar\omega \quad (21)$$

Where E_{Fc} and E_{Fv} are the quasi-Fermi energies for electrons in the condition band and holes in the valence band, respectively and $\hbar\omega$ is the lasing frequency of the laser diode.

In GaAs inner layer where stimulated emission takes place is called the active region. To maintain the lasing action of the gain medium, it is necessary to confine the light as tightly as possible to the active region. Since the walk away modes does not contribute to the gain. This confinement can be achieved by dielectric waveguiding effect due the dielectric constant differences between the gain medium and the barrier regions. When the optical mode is confined to the active region the diode laser lases at frequency ω with photon energy,

$$\hbar\omega = E_{Fc} - E_{Fv} \quad (22)$$

We know that the effect of the oscillating driving field causes the bound state to be sifted by a significant energy value to form a quasibound state. The gain region under the effect of oscillating deriving field would cause the energy difference between the quasi-Fermi energy levels for electrons and holes to widen out. Thus, the laser frequency tuned to higher frequency values which changes the laser diode output frequency,

$$\hbar\omega' = E'_{Fc} - E'_{Ev} \quad (23)$$

Where ω' is the new lasing frequency and E'_{Fc} and E'_{Ev} are the new quasi-Fermi energy levels for electron in the condition band and for hole in the valence band, respectively, under the presence of the external oscillating driving field. Another possible refinement of the laser operations is to lower the laser linewidth and increasing its monochromaticity. This happens, when the electrons piled in the quasibound state, but according the system parameters this pile of electrons can be sharp or wide over a significant energy interval, (Fig. 4b and 5b). For a good laser operation it is desirable to confine electrons in a very narrow energy band. This confinement would lead to lower laser linewidth and would increase the monochromaticity of the laser diode output. The laser intensity can be controlled by controlling the number of electrons can be trapped in the quasibound state. Once the laser diode is fabricated we can not control the effective masses of the well or the barrier regions. In Fig. 5b, the controlling factor of the height and width of the quasibound state is the oscillating field amplitude V_1, the quasibound state has almost the same position in energy which means the lasing frequency would not change significantly with changing the field amplitude but the intensity is.

CONCLUSIONS

We developed Floquet scattering theory to determine the scattering matrix, S-matrix, for oscillating quantum well driven by external field. Numerically solving the S-matrix, we were able to determine the quasibound state induced because of the oscillating driving field and the profile of the electron accumulation in the quasibound state. Also, with the aid of the numerical code, we were able to study the effect of the system parameter of the transmission amplitude. The most important parameters of the system are the field energy and field amplitude since we can control but the physical parameters of the semiconductor diode we can not once the device is fabricated. This shift in the bound state energy is used to tune the lasing frequency and the output laser line width of the semiconductor laser by changing the deriving field frequency and amplitude.

ACKNOWLEDGMENT

The author wishes to thanks Dr. Ahmed El-Tayyan for a helpful discussion and fine comments on the subject of this study.

REFERENCES

Al-Sahhar, Z.I., M.M. Shabat, H.S. Ashour, 2005. Floquet scattering through a time-periodic potential for a position-dependent electron effective mass structure. The First International Conference for Science and Development, The Islamic University of Gaza-Palestine, 1-2 March (2005), Gaza, Palestine.

Büttiker, M., 1986. Role of quantum coherence in series resistors. Phys. Rev. Lett., 57: 1761.

Chow, K. and III. Sargent, 1994. Semiconductor Laser Physics. Springer-Verlag.

Chuang, S.L., 1995. Physics of Optoelectronic Devices. Wiley Series in Pure and Applies Physics.

Durate, F.J. and J.A. Piper, 1980. A double-prism bean expander for pulsed dye laser. Opt. Commun., 35: 100-104.

Durate, F.J. and J.A. Piper, 1981. Prism preexpanded grazing-incidence grating cavity for pulsed dye lasers, Applied Opt., 21: 2113-2116.

Durate, F.J. and J.A. Piper, 1984. Narrow-linewidth, high prf copper laser-pumped dye-laser oscillators. Applied Opt., 23: 1391-1394.

Hong, J., H. Kim and T. Makino, 1998. Enhanced wavelength tuning range in two-section complex-coupled DFB lasers byalternating gain and loss coupling. IEEE J. Light. Technol., 16: 1323-1328.

Jerman, J.H., J.D. Grade, J.D. Berger and J.H. Heanue, 2001. Tunable laser with microactuator. Intl. Pub. WO 01/43241, June.

Landauer, R., 1989. Conductance determined by transmission: probes and quantised constriction resistance. J. Phys., Condend. Matter, 1: 8099.

Littman, M.G. and H.J. Metcalf, 1978. Spectrally narrow pulsed dye laser without beam expander. Applied Opt., 17: 2224-2227.

Littman, M.G., 1984. Single-mode pulsed tunable dye laser. Applied Opt., 23: 4465-4468.

Mason, B., G.A. Fish, S.P. DenBaars and L.A. Coldren, 1999. Widely tunable sampled grating DBR laser with integrated electroabsorption modulator. Photon. Tech. Lett., 11: 638-640.

Moskalets, M. and M. Büttiker, 2002a. Floquet states and persistent currents transitions in a mesoscopic ring. arXiv:cond-mat/0207258 v1 10July.

Moskalets, M. and M. Büttiker, 2002b. Floquet scattering theory of quantum pumps. arXiv:cond-matt/0208356 v1 19 Aug 2002.

Peterson, O.G., S.A. Tuccio and B.B. Snavely, 1970. CW operation of an organic dye solution laser Applied Phys. Lett., 17: 245-247.

Schafer, F.P., W. Schmidt and J. Volze, 1966. Organic dye solution laser. Applied Phys. Lett., 9: 306-309.

Shoshan, I., N.N. Danon and U.P. Oppenheim, 1997. Narrowband operation of a pulsed dye laser without intracavity beam expansion. J. Applied Phys., 48: 5595-4497

Sorokin, P.P. and J.R. Lankard, 1966. Stimulated emission obseverd from an organic dye, chloro-aluminum phthalocyanine. IBM J. Res. Develop., 10: 162-163.

Tang, C.S., Y.H. Tan and C.S. Chu, 2003. Transport spectroscopy in a time-modulated open quantum dot. Phys. Rev. B., 67: 205324-205331.

Vakhshoori, D., P. Tayebati, C.C. Lu, M. Azimi, P. Wang, J.H. Zhou and E. Canoglu, 1999. 2 mW CW single modeoperation of a tunable 1550 nm vertical cavity surface emitting laser with 50 nm tuning range. Electron. Lett., 35: 1-2.

Verdeyen, J.T., 1995. Laser Electronics, 3rd Edn., Prentice Hall.

Wenjun, L. and L.E. Reichl, 1999. Floquet scattering through a time periodic potential. Phys. Rev. B., 60: 15732.

Wenjun, L. and L.E. Reichl, 2000. Transport in strongly driven heterostructures and bound state induced dynamic resonances. Phys. Rev. B., 62: 8269.

Yariv, A., 1989. Quantum Electronics. 3rd Edn., Wiley.

Zorabedian, P., 1995. Tunable External Cavity Semiconductor Lasers. in Tunable Laser Handbook. Duarte, F.J. (Ed.), Academic Press, San Diego.